Proceedings of the 5th International Conference on Civil Engineering for Sustainable Development (ICCESD 2020), 7~9 February 2020, KUET, Khulna, Bangladesh (ISBN-978-984-34-8764-3)

CHANGE IN TRANSVERSE SLOPE OF WATER SURFACE AT RIVER BEND: A NUMERICAL STUDY

Priyata Rahman *[1], MD. Shahjahan Ali[2]

[1] *Postgraduate Student, Institute of Disaster Management, Khulna University of Engineering & Technology, Bangladesh. e-mail: priyata2214.pr@gmail.com*
[2] *Professor, Department of Civil Engineering, Khulna University of Engineering & Technology, Bangladesh, e-mail: babul41@yahoo.com*

***Corresponding Author**

ABSTRACT

In recent years, the CFD (Computational Fluid Dynamics) models application is considered to be efficient tool to study the river processes and outdoor channels. Generation of secondary current in a meandering river flow due to the centrifugal force acting on the river is obviously three dimensional (3D) in nature. But in case of practical problems like alluvial geomorphic processes, 3D models are not proved to be efficient. Hence, two dimensional (2D) models are generally adopted for such problems. This study offers a presentation of numerical simulation results for turbulent flows around bends of a meandering channel for different meander angles. 2D models were built by the use of iRIC Nays2DH for flow simulation for 45˚, 90˚, 135˚, 180˚ meandering bends with varying widths of 0.15m, 0.25m, 0.75m, 1.00m, 1.25m, 1.50m considering constant Froude number, with constant meandering length (M_L/W) and constant radius of curvature (R/W). Zero equation model was used as turbulence closure model with finite differential advections as upwind scheme. The flow behavior had been studied at the apex and cross over portions of bends. From the simulation, the velocity at outer bank was found to be lower than that of the inner bank while the water surface elevation was found to be higher than that of the inner bank. Increase in transverse slope of water surface at bend was observed for increasing meander angles, Froude numbers and decreasing channel widths. The simulation of flow at bend of meandering channel was successfully carried out by using iRIC Nays2DH.

Keywords: *Meandering river, two dimensional flow, bend, channel width, Froude number, iRIC, Nays2DH.*

1 INTRODUCTION

The classification of river includes a large number of classes. They can be classified according to topography of river basin, flood hydrograph, origin, discharge, sinuosity etc. The term sinuosity describes an index which is used to elaborate the channel platform. It is mainly defined as the ratio of channel length to straight line distance of the river. In general, rivers of a straight planform having sinuosity value of 1, are uphill to find and are rare in nature. Most of the rivers in general are of meandering pattern which is most common in the river morphology. By the term meandering pattern it concludes rivers having a sinuosity value greater than 1.5, holding alternate bends. They are generated by the combined actions of the sediment transport in rivers and the water flow. The water flow simulation in meandering river has been a popular topic for research work purpose in river engineering and water resources engineering field. Flow through bends includes three dimensional (3D) patterns as secondary current is produced in a meandering river. When flow approaches to bends, water current flows from the convex side towards the concave. This phenomenon is mainly created by the centrifugal forces acting on the water. In contrast, the water surface in the outer bank rises and makes the inner bank lower thus balances the centrifugal force acting on water surface. Thus produces variation in flow rate along different portion of the river. This elevation change between the outer and inner banks creates transverse slope in water surface. The study of such a flow involves 3D hydrodynamic model. But for the practical application like the alluvial geomorphic processes, the 3D model does not provide much efficiency. For this reason, generally two-dimensional (2D) model is adopted to simulate the flow in a meandering river. The study and analysis of flow through meandering channels hold extensive interest in the field of river engineering for the construction of flood retention structures as rivers play a vital role in influencing the environment. Meandering rivers are formed when sediment erosion occurs, comprising an outer concave bank which is followed by deep scour holes and deposition of sediments are executed on an inner convex curve at downstream creating shallow depth. The creation of inner bank is encouraged by the development of vegetation at low flow stages and consequently stabilizing the point bar (the submergence of zone of minimum flow depth). And the transport of sediments from the outer bank to the inner bank brings changes in the shape of the river. Thus enhances the creation of meander channels. The continuous migration of meander channels can be a reason of many practical problems such as bank erosion, shifting of center line and boundaries, loss of fertile soil, heterogeneous sediment stratigraphy etc.

In the past, many researchers have taken initiative to explain the flow pattern in a meander by considering different meander angles and discharges with varying geometric conditions. Kim and Choi (2003) performed an experiment to simulate the open channel flows in meandering bend. By considering the finite element method they evaluated the 2D numerical algorithm to complete the simulation. Rozovskii (1961) considered a completely smooth and rough bed of a rectangular channel with 180˚ meander bends where the channel width was taken to be 80 cm and the radius of curvature for the 180˚ bend was 80 cm on the centerline. A value for discharge was taken to be 12.3 l/sec while the flow depth, Froude number and Reynolds number were chosen as 5.8 cm, 0.35 and 14000 respectively. He conducted an exploration for trapezoidal channels also. He gave an extensive discussion on the flow mechanism of the meander and explained the generation of secondary current through bends and also interpreted the change of tangential secondary current of flow while traversing a bend. A numerical model in harmony of Rozovskii tests was formed by Leschziner and Rodi (1974) for a 90˚ strongly curved bend where the ratio of average radius to width was considered as 1. In this research, he found the external bank surface slope to be lower than the inner bank surface slope and did not get a linear surface slope along the cross section. De Vriend and Geoldof (1983) constructed a model with 90˚ central angle, 6m channel width, 0.25m channel depth, 0.25 Froude number, 50m radius of curvature with a discharge value of 0.61 m^3/sec. From this hypothesis, the surface transversal profile was found to be linear but the calculation of water surface elevation along the upstream and downstream bends were not done. Ali *et al.*, (2017) worked on the flow pattern around a bend in an open channel for different bend angles of 45˚, 90˚, 135˚ and 180˚. The simulation was done by using the iRIC software. Sharply and mildly curved channels were constructed for predicting the

simulation of the flow field. Constant discharge at upstream and constant depth with zero velocity gradients was given as downstream boundary conditions. The length of the high velocity zone in inner bank and low velocity zone in outer bank along stream-wise direction was found higher for 135˚ bend and gradually decreasing with the decrease of bend angle. Ahmadi *et al.* (2009) worked on a 2D depth-average model for simulating the unsteady flow norms in bends of an open channel. The impression of the secondary flow occurrence was considered in the calculation of dispersion stresses. The actual and mean velocity distributions are inconsistent. Due to which, the product integration is generated and influence the creation of dispersion stresses. These phenomena are considered while performing the momentum equation. In the experiment, orthogonal curvilinear co-ordinate system was used for the simulation of flow with irregular boundary conditions. Finite volume projection method was used in case of staggered grid for evolving the governing equation. They concluded the experimental results by showing a good arrangement of the water surface elevation measurements. They also illustrated a good simulation result with improved dispersion terms.

Due to the generation of secondary current of flow in a meandering channel because of the effect of centrifugal force acting on the water surface, the flow through bends involve three dimensional flow nature. But for the application in the practical engineering problems such as- alluvial geomorphic processes, generally two dimensional models are evaluated to get proper efficiency level of the work. In this study, a 2D model based software named iRIC Nays2DH is used for the simulation of flows for bend angles of 45˚, 90˚, 135˚ and 180˚ considering channels widths of 0.15m, 0.25m, 0.50m, 0.75m, 1.00m, 1.25m and 1.50m of the river and for Froude number of 0.25 and 0.50.

2 SIMULATION TECHNIQUE

In this study the iRIC Nays2DH software is used to simulate the flow fields. The iRIC software provides a vast scope for evaluating the flow in a domain such as- transport of sediment, evaluation of bed, two and three dimensional flow simulation, processing of topographic data, ground-surface-water interrelation, assessment of dwelling, model output visualization, editing tools, mapping, extracting data etc (Shimizu & Takebayashi, 2014). This software is made suitable for exploiting the sets of river data from the river reaches. An advantage is that a user can readily use the software as the models are adorned with single graphical user interface and hence there is no need for the user to learn the pre and post processing tools. This approach is made available for the users by supporting all documentation in public domain. Nays2DH comprises an analytical model for the simulation of two-dimensional (2D) horizontal flow, morphological variation of beds and banks of river, transport of sediment. The basic equations used in this model are obtained from the transformation of the basic equations in an orthogonal co-ordinates system (x, y) into a general curvilinear co-ordinate system as follows.

Continuity Equation

$$\frac{\partial}{\partial t}\left(\frac{h}{J}\right)+\frac{\partial}{\partial \xi}\left(\frac{hu^{\xi}}{J}\right)+\frac{\partial}{\partial \eta}\left(\frac{hu^{\eta}}{J}\right)=0$$

Momentum Equations

$$\frac{\partial u^{\xi}}{\partial t}+u^{\xi}\frac{\partial u^{\xi}}{\partial \xi}+u^{\eta}\frac{\partial u^{\eta}}{\partial \eta}+\alpha_1 u^{\xi}u^{\xi}+\alpha_2 u^{\xi}u^{\eta}+\alpha_3 u^{\eta}u^{\eta}$$
$$=-g\left[(\xi_x^2+\xi_y^2)\frac{\partial H}{\partial \xi}+(\xi_x\eta_x+\xi_y\eta_y)\frac{\partial H}{\partial \eta}\right]$$
$$-\left(C_f+\frac{1}{2}C_D\alpha_s h\right)\frac{u^{\eta}}{hJ}\sqrt{(\eta_y u^{\xi}-\xi_y u^{\eta})^2+(-\eta_x u^{\xi}-\xi_x u^{\eta})^2}+D^{\eta}$$

$$\frac{\partial u^{\xi}}{\partial t} + u^{\xi}\frac{\partial u^{\xi}}{\partial \xi} + u^{\eta}\frac{\partial u^{\eta}}{\partial \eta} + \alpha_4 u^{\xi}u^{\xi} + \alpha_5 u^{\xi}u^{\eta} + \alpha_6 u^{\eta}u^{\eta}$$
$$= -g\left[(\eta_x\xi_x + \eta_y\xi_y)\frac{\partial H}{\partial \xi} + (\eta_x^2 + \eta_y^2)\frac{\partial H}{\partial \eta}\right]$$
$$-\left(C_f + \frac{1}{2}C_D\alpha_s h\right)\frac{u^{\eta}}{hJ}\sqrt{(\eta_y u^{\xi} - \xi_y u^{\eta})^2 + (-\eta_x u^{\xi} - \xi_x u^{\eta})^2} + D^{\eta}$$

Where,

$\alpha_1 = \xi_x\frac{\partial^2 x}{\partial \xi^2} + \xi_y\frac{\partial^2 y}{\partial \xi^2}$, $\alpha_2 = 2\left(\xi_x\frac{\partial^2 x}{\partial \xi \partial \eta} + \xi_y\frac{\partial^2 y}{\partial \xi \partial \eta}\right)$, $\alpha_3 = \xi_x\frac{\partial^2 x}{\partial \eta^2} + \xi_y\frac{\partial^2 y}{\partial \eta^2}$

$\alpha_4 = \eta_x\frac{\partial^2 x}{\partial \xi^2} + \eta_y\frac{\partial^2 y}{\partial \xi^2}$, $\alpha_5 = 2\left(\eta_x\frac{\partial^2 x}{\partial \xi \partial \eta} + \eta_y\frac{\partial^2 y}{\partial \xi \partial \eta}\right)$, $\alpha_6 = \eta_x\frac{\partial^2 x}{\partial \eta^2} + \eta_y\frac{\partial^2 y}{\partial \eta^2}$

$D^{\xi} = \left(\xi_x\frac{\partial}{\partial \xi} + \eta_x\frac{\partial}{\partial \eta}\right)\left[v_t\left(\xi_x\frac{\partial u^{\xi}}{\partial \xi} + \eta_x\frac{\partial u^{\eta}}{\partial \eta}\right)\right] + \left(\xi_y\frac{\partial}{\partial \xi} + \eta_y\frac{\partial}{\partial \eta}\right)\left[v_t\left(\xi_y\frac{\partial u^{\xi}}{\partial \xi} + \eta_y\frac{\partial u^{\eta}}{\partial \eta}\right)\right]$

$D^{\eta} = \left(\xi_x\frac{\partial}{\partial \xi} + \eta_x\frac{\partial}{\partial \eta}\right)\left[v_t\left(\xi_x\frac{\partial u^{\eta}}{\partial \xi} + \eta_x\frac{\partial u^{\eta}}{\partial \eta}\right)\right] + \left(\xi_y\frac{\partial}{\partial \xi} + \eta_y\frac{\partial}{\partial \eta}\right)\left[v_t\left(\xi_y\frac{\partial u^{\eta}}{\partial \xi} + \eta_y\frac{\partial u^{\eta}}{\partial \eta}\right)\right]$

$\xi_x = \frac{\partial \xi}{\partial x}$, $\xi_y = \frac{\partial \xi}{\partial y}$, $\eta_x = \frac{\partial \eta}{\partial x}$ $\eta_y = \frac{\partial \eta}{\partial y}$

$u^{\xi} = \xi_x u + \xi_y v, u^{\eta} = \eta_x u + \eta_y v$ b

$J = \frac{1}{x_\xi y_\eta - x_\eta y_\xi}$

$k - \varepsilon$ model is used for turbulent closure. In the standard $k - \varepsilon$ model, the eddy viscosity co-efficient can be evolved by the following expression-

$$v_t = C_\mu\frac{k^2}{\epsilon}$$

Where, C_μ= model constant,

k and ϵ are attained by the following equations-

$$\frac{\partial k}{\partial t} + u\frac{\partial k}{\partial t} + v\frac{\partial k}{\partial t} = \frac{\partial}{\partial x}\left(\frac{v_t}{\sigma_k}\frac{\partial k}{\partial x}\right) + \frac{\partial}{\partial y}\left(\frac{v_t}{\sigma_k}\frac{\partial k}{\partial y}\right) + P_h + P_{kv} - \epsilon$$

$$\frac{\partial \epsilon}{\partial t} + u\frac{\partial \epsilon}{\partial t} + v\frac{\partial \epsilon}{\partial t} = \frac{\partial}{\partial x}\left(\frac{v_t}{\sigma_\epsilon}\frac{\partial \epsilon}{\partial x}\right) + \frac{\partial}{\partial y}\left(\frac{v_t}{\sigma_\epsilon}\frac{\partial \epsilon}{\partial y}\right) + C_{1_\epsilon}\frac{\epsilon}{k}P_h + P_{\epsilon v} - C_{2_\epsilon}\frac{\epsilon^2}{k}$$

Table 1: Model constants.

C_μ	C_{1_ϵ}	C_{2_ϵ}	σ_k	σ_ϵ
0.09	1.44	1.92	1.00	1.30

Where, C_{1_ϵ}, C_{2_ϵ}, σ_k and σ_ϵ are the model constants having the particular values given in Table 1.

The terms P_{kv} and $P_{\epsilon v}$ are obtained by-

P_{kv}= $C_k\frac{u_*^3}{h}$ = 0.33

$$P_{\epsilon v} = C_k \frac{u_*^4}{h^2}$$

2.1 Numerical test cases

The hydraulic parameters for numerical test cases that were adopted in this study for flow simulation are given in Table 2. Figure 1 shows the meander geometry for series S_1. In the simulation cases, the width of the channel varies from 0.15 to 1.50m and meander length varies from 4.5 to 45m having a constant meandering length M_L/W =30 and for a constant radius of curvature R/W=7.5. 56 numbers of numerical test cases for flow simulations were run within the seven series (S_1 to S_7) of numerical test cases as shown in Table 3. The simulations were performed for bend angles of 45˚, 90˚, 135˚ and 180˚ and for Froude number of 0.25 and 0.50.

Table 2: Meander parameters.

Series No.	Width of Channel, w (m)	Meander Length, M_L (m)	$\frac{M_L}{w}$	Meander Belt (m)	Length of Channel (m)	Radius of Curvature R, (m)
S_1	0.15	4.5	30	2.41	12	1.13
S_2	0.25	7.5	30	4.01	20	1.88
S_3	0.50	15.0	30	8.00	40	3.75
S_4	0.75	22.5	30	12.01	60	5.63
S_5	1.00	30.0	30	16.00	80	7.50
S_6	1.25	37.5	30	20.01	100	9.38
S_7	1.50	45.0	30	24.00	120	11.25

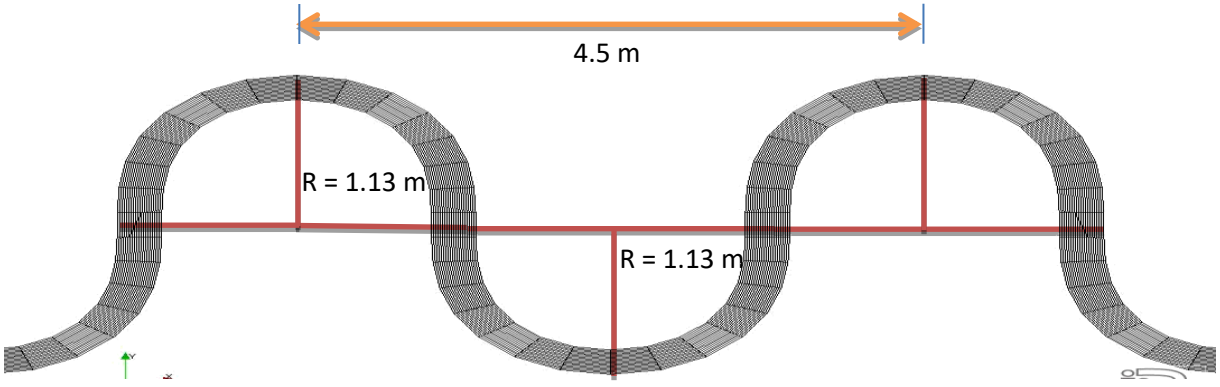

Figure 1: Meander geometry for series S_1.

Table 3: Hydraulic parameters for numerical test cases.

Series No.	Case No.	Bend Angle	Fr	Width of Channel (m)	Discharge, Q (m^3/s)
S_1	$S_1C_1R_1 \sim S_1C_1R_4$	45˚, 90˚, 135˚, 180˚	0.25	0.15	0.05459
	$S_1C_2R_1 \sim S_1C_2R_4$	45˚, 90˚, 135˚, 180˚	0.50	0.15	0.10918
S_2	$S_2C_1R_1 \sim S_2C_1R_4$	45˚, 90˚, 135˚, 180˚	0.25	0.25	0.09098
	$S_2C_2R_1 \sim S_2C_2R_4$	45˚, 90˚, 135˚, 180˚	0.50	0.25	0.18195
S_3	$S_3C_1R_1 \sim S_3C_1R_4$	45˚, 90˚, 135˚, 180˚	0.25	0.50	0.18196
	$S_3C_2R_1 \sim S_3C_2R_4$	45˚, 90˚, 135˚, 180˚	0.50	0.50	0.36390
S_4	$S_4C_1R_1 \sim S_4C_1R_4$	45˚, 90˚, 135˚, 180˚	0.25	0.75	0.27294
	$S_4C_2R_1 \sim S_4C_2R_4$	45˚, 90˚, 135˚, 180˚	0.50	0.75	0.54585
S_5	$S_5C_1R_1 \sim S_5C_1R_4$	45˚, 90˚, 135˚, 180˚	0.25	1.00	0.36392
	$S_5C_2R_1 \sim S_5C_2R_4$	45˚, 90˚, 135˚, 180˚	0.50	1.00	0.72780
S_6	$S_6C_1R_1 \sim S_6C_1R_4$	45˚, 90˚, 135˚, 180˚	0.25	1.25	0.45490
	$S_6C_2R_1 \sim S_6C_2R_4$	45˚, 90˚, 135˚, 180˚	0.50	1.25	0.90975
S_7	$S_7C_1R_1 \sim S_7C_1R_4$	45˚, 90˚, 135˚, 180˚	0.25	1.50	0.54588
	$S_7C_2R_1 \sim S_7C_2R_4$	45˚, 90˚, 135˚, 180˚	0.50	1.50	1.09170

Here, in Table 3, R_1, R_2, R_3 and R_4 represents simulation run for 45˚, 90˚, 135˚ and 180˚ bend angles of meanders, respectively. S_1, S_2, S_3, S_4, S_5, S_6 and S_7 stands for the series numbers having channel widths of 0.15m, 0.25m, 0.50m, 0.75m, 1.00m, 1.25m and 1.50m, respectively. C_1 and C_2 are the cases of simulation for Froude numbers of 0.25 and 0.50.

3 RESULTS AND DISCUSSIONS

The meander length of models varied with channel widths, as the ratio of meander length to width of the channel was taken to be a constant value of 30. Number of grids in the longitudinal and transverse direction was 161 and 21 respectively. At the sidewall locations, the logarithmic law was encountered in the numerical solution. Boundary conditions were set up by inserting a constant discharge at upstream and a constant depth at the downstream end. Seven sections of 1-1, 2-2, 3-3, 4-4, 5-5, 6-6 and 7-7 were considered as illustrated in Figure 2.

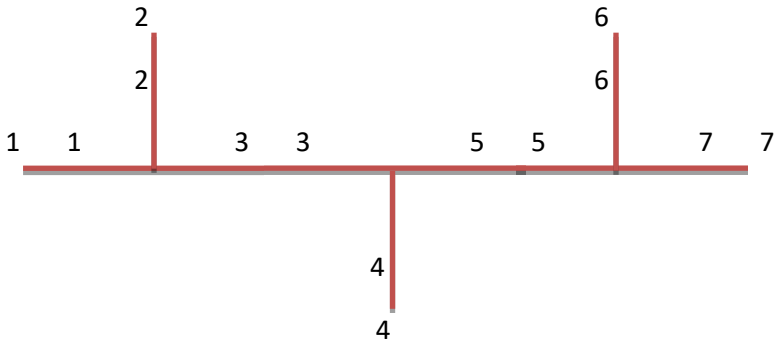

Figure 2: Sections taken for simulation.

3.1 Simulated Flow Profiles

Figure 3 shows that the value of depth was high for the outer concave end in comparison with the inner convex end and the center of the channel. Thus it developed a transverse water surface slope. And from the velocity vectors in Figure 3, it is evident that the velocity vectors were high in inner convex end and low in outer concave end. The value range of water surface elevation was higher for higher Froude number (0.50) than lower Froude number (0.25).

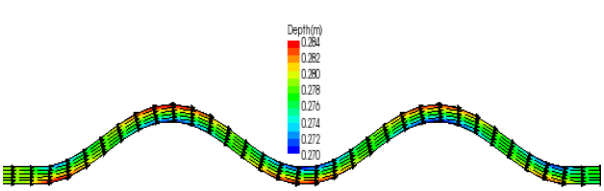

(a) (Case $S_1C_1R_1$).

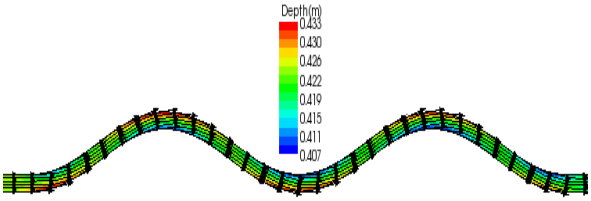

(b) (Case $S_1C_2R_1$).

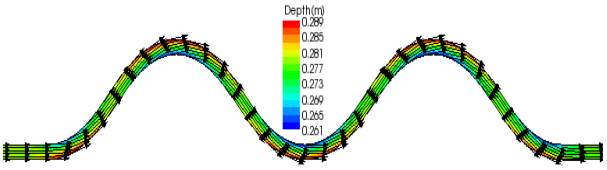

(c) (Case $S_1C_1R_2$).

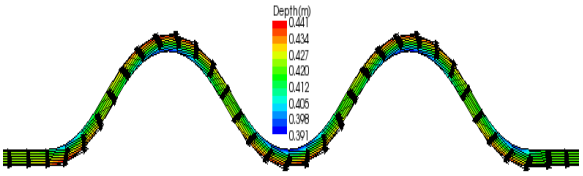

(d) (Case $S_1C_2R_2$).

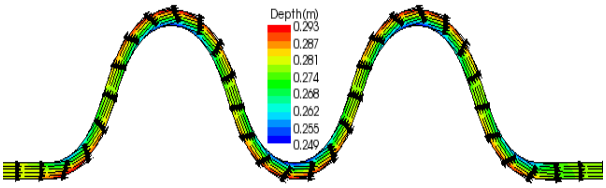

(e) (Case $S_1C_1R_3$).

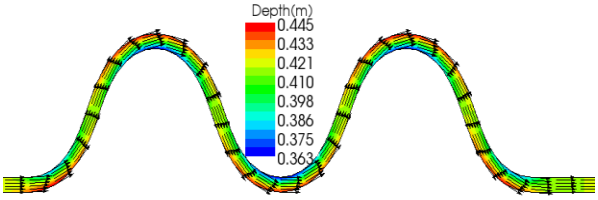

(f) (Case $S_1C_2R_3$).

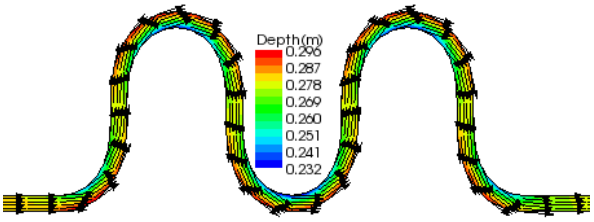

(g) (Case $S_1C_1R_4$).

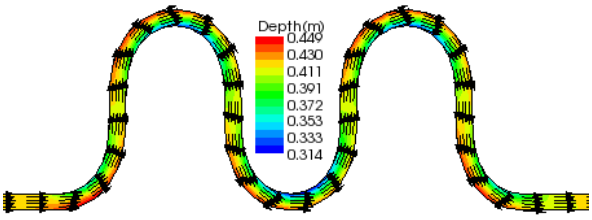

(h) (Case $S_1C_2R_4$).

Figure 3: Simulated velocity vectors superimposed with depth contour for cases $(S_1C_1R_1 \sim S_1C_1R_4)$ and $(S_1C_2R_1 \sim S_1C_2R_4)$.

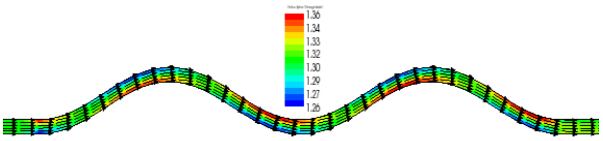

(a) (Case $S_1C_1R_1$).

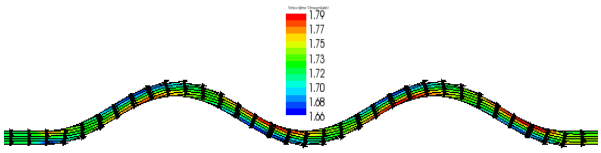

(b) (Case $S_1C_2R_1$).

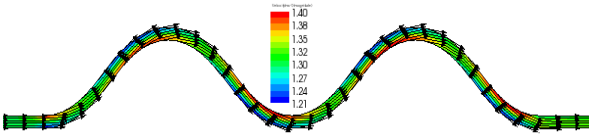

(c) (Case $S_1C_1R_2$).

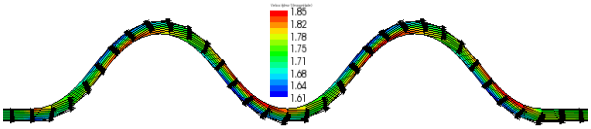

(d) (Case $S_1C_2R_2$).

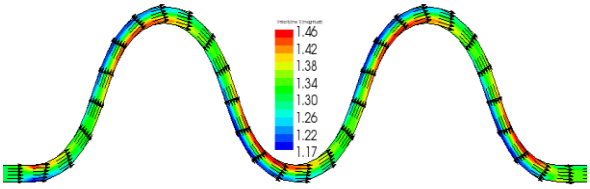

(e) (Case $S_1C_1R_3$).

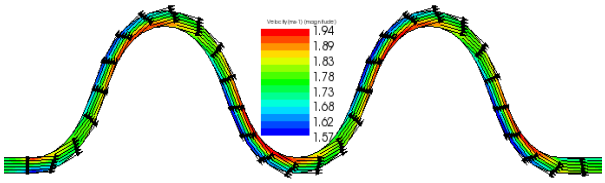

(f) (Case $S_1C_2R_3$).

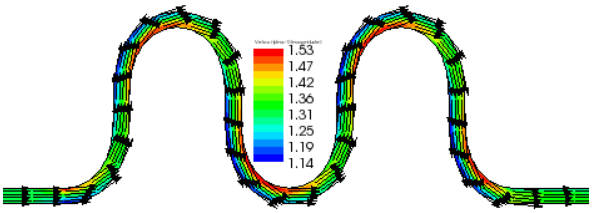

(g) (Case $S_1C_1R_4$).

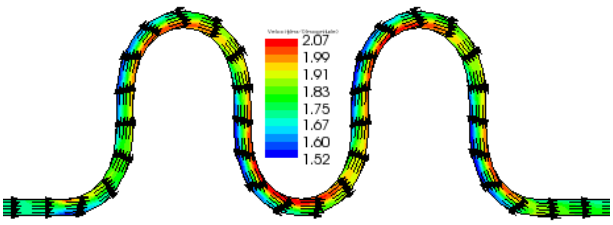

(h) (Case $S_1C_2R_4$).

Figure 4: Simulated velocity vectors superimposed with velocity contour for cases ($S_1C_1R_1$~$S_1C_1R_4$) and ($S_1C_2R_1$~$S_1C_2R_4$).

Figure 4 shows that the velocity in the outer bank was lower while the velocity at the inner bank was higher. The velocity at the center of the channel was higher than that of the velocity magnitude at the outer bank. And from the velocity vectors in Figure 4, it is evident that the velocity vectors were high in inner convex end and low in outer concave end. The value range of velocity magnitude was higher for 0.50 Fr number than 0.25 Fr number.

3.2 Transverse Slope in Water Surface

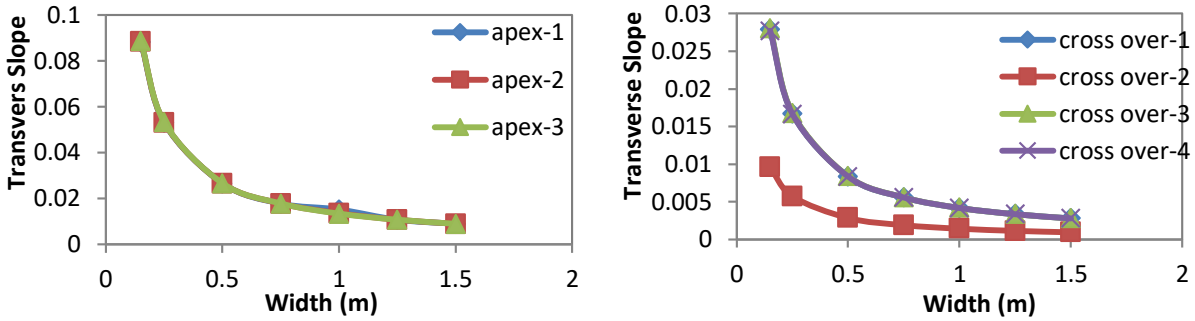

(a) $(S_1C_1R_1 \sim S_7C_1R_1)$. (b) $(S_1C_1R_1 \sim S_7C_1R_1)$.

Figure 5: Transverse slope at apex points and cross-over points for different values of widths having meandering length (M_L/W), Radius of Curvature (R/W) and Froude numbers are constant.

From Figure 5, it was found that the transverse slope of water surface at the cross over sections of a meander was lower than that of the apex points The transverse slope was found to decrease with the increase of width of the channel. It was found out that the change in transverse slope of water surface varied rapidly for channel widths between (0.15-0.75)m while the change in transverse slope was gradual for width of channel greater than 0.75m.

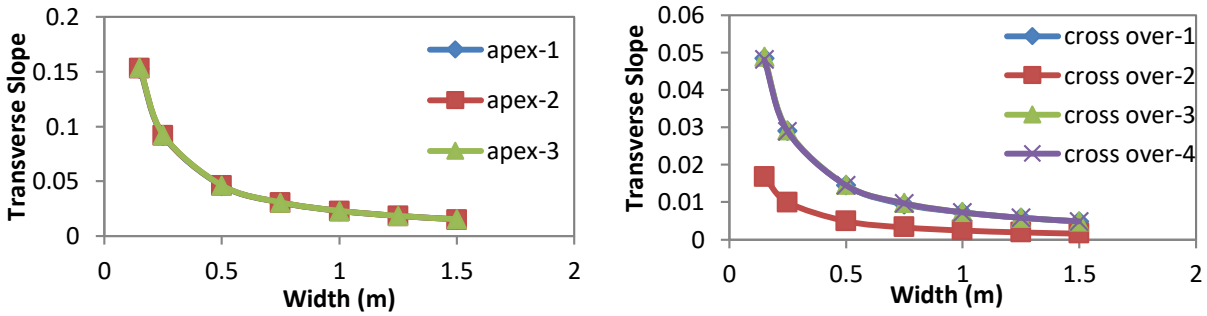

(a) $(S_1C_2R_1 \sim S_7C_2R_1)$. (b) $(S_1C_2R_1 \sim S_7C_2R_1)$.

Figure 6: Transverse slope-width graph at apex points and cross over points of meander bend.

Figure 6 shows that the transverse slope of water surface at the cross over points of a bend was lower than that of the apex points. The transverse slope was found to decrease with the increase of width of the channel. It was found out that the change in transverse slope of water surface varied rapidly for channel widths between (0.15-0.75)m while the change in transverse slope was gradual for width of channel greater than 0.75m.

It was also observed that the transverse slope of water surface at the apex points and cross over points of a meander bend for Froude number 0.50 was higher than that of the transverse slope of water surface with Froude number value of 0.25.

Table 4 shows the value range of transverse slope of water surface for the numerical test cases that were run for simulation of flow.

Table 4: Change in transverse slope of water surface for different test cases.

Case No.	At apex point-1	At apex point-2	At apex point-3	At cross over point-1	At cross over point-2	At cross over point-3	At cross over point-4
$S_1C_1R_1$ ~ $S_7C_1R_1$	0.0881 ~ 0.00883	0.08835 ~ 0.00884	0.08856~ 0.00885	0.0279 ~ 0.0028	0.00961~ 0.00095	0.02803~ 002795	0.02771~ 0.00278
$S_1C_2R_1$ ~ $S_7C_2R_1$	0.15269 ~ 0.01536	0.15337 ~ 0.15337	0.15394 ~ 0.0154	0.04842 ~ 0.00485	0.01679 ~ 0.00165	0.0488 ~ 0.00486	0.04804 ~ 0.00483
$S_1C_1R_2$ ~ $S_7C_1R_2$	0.17873 ~ 0.01771	0.17962 ~ 0.01776	0.17998 ~ 0.01784	0.05581 ~ 0.00553	0.01921 ~ 0.00189	0.05613 ~ 0.00556	0.05555 ~ 0.00554
$S_1C_2R_2$ ~ $S_7C_2R_2$	0.31267 ~ 0.03077	0.31457 ~ 0.03089	0.31494 ~ 0.03107	0.09763 ~ 0.00957	0.03385 ~ 0.00326	0.09826 ~ 0.00965	0.0966 ~ 0.00961
$S_1C_1R_3$ ~ $S_7C_1R_3$	0.27699 ~ 0.02672	0.27901 ~ 0.0269	0.27879 ~ 0.02714	0.08439 ~ 0.00816	0.02903 ~ 0.00278	0.08478 ~ 0.00825	0.08388 ~ 0.00827
$S_1C_2R_3$ ~ $S_7C_2R_3$	0.49898 ~ 0.04635	0.50246 ~ 0.04678	0.49752 ~ 0.04737	0.15123 ~ 0.01406	0.05234 ~ 0.00481	0.15121 ~ 0.01431	0.14703 ~ 0.01431
$S_1C_1R_4$ ~ $S_7C_1R_4$	0.36906 ~ 0.03586	0.39402 ~ 0.03631	0.39139 ~ 0.03688	0.11405 ~ 0.01063	0.0392 ~ 0.00361	0.11439 ~ 0.01082	0.11302 ~ 0.01093
$S_1C_2R_4$ ~ $S_7C_2R_4$	0.72637 ~ 0.0619	0.74847 ~ 0.06297	0.73319 ~ 0.06438	0.20847~ 0.01814	0.07385~ 0.01866	0.22014 ~ 0.01866	0.20205~ 0.01883

4 CONCLUSIONS

The flow fields of the channels with 45˚, 90˚, 135˚ and 180˚ bend angles with 0.15m, 0.25m, 0.50m, 0.75m, 1m, 1.25m and 1.5m channel widths were successfully simulated by using the two dimensional flow simulation software of iRIC Nays2DH. The changes of transverse slope, velocity and water surface elevation due to different geometric conditions of the channels were found out by using this software. The simulation results showed that the water surface elevation at the outer bank was higher than the inner bank. From the velocity profiles, it was observed that velocity at outer bank was lower than the inner bank. It is found that, there is an increase in transverse slope of water surface due to the increase in meandering angles and Froude numbers while it decreased with increasing channel widths having meandering length (M_L/W), Radius of Curvature (R/W) and Froude numbers are constant. It was also observed that the transverse slope of water surface at the apex and cross over points of a meander was higher for Froude number 0.50 than that of the transverse slope of water surface with Froude number value of 0.25. It can be concluded that the iRIC Nays2DH software is suitable for simulating the flow field at bends and as well as at straight portions.

REFERENCES

Ahmed, M. M., Ayyoubzadeh, S.A., Namin, M. M. and Samani, J.M.V. (2009). "A 2D depthaveraged model for simulating and examining unsteady flow patterns in open channel bend". Department of Water Structures Engineering, College of Agriculture, Tarbiat Modares University, P.O. Box: 14115-336, Tehran, Islamic Republic of Iran.

Ali, M. S. Lemon, M. H. R., and Talukder, M. A. Q. (2014) "Two dimensional simulation of flows in bends of an open channel by iRIC Nays2D", Proceedings of the 2nd International Conference on Civil Engineering for Sustainable Development (ICCESD-2014), 14~16 Feb., KUET, Bangladesh, pp. 103-104 of Ext. Abstract Proc. (Full paper in CD-ROM).

De-Vriend, H.J. and H.J. Geoldof, (1983). "Main flow velocity in Short River bends". Journal of Hydraulic Engineering, ASCE, 109: 991-1011.

Kim, T.B. and Choi, S.U. (2003). "Experiment on numerical simulations of open-channel flows in a bend using the finite element method". School of Civil and Environmental Engineering, Yonsei University, Seoul, Korea.

Leschziner, M.A. and Rodi, W. (1979). "Calculation of strongly curved open channel flow". Journal of Hydraulic Engineering, ASCE, 105: 1297-1314.

Rozovskii, I.L. (1961). "Flow of water in bends of open channels". Academy of Sciences of the Ukrainian SSR, Kiev, Israel Program for Scientific Translation, Jerusalem.

Science, C. R. (2014) 'iRIC Software Nays2DH Solver Manual'.

Shimizu, Y. and Takebayashi, H. (2014). "iRIC software Nays2DH solver manual", Nays2DH development team, Japan.